Measurements of Ionic Structure in Shock Compressed Lithium Hydride from Ultrafast X-Ray Thomson Scattering

A. L. Kritcher,[1,2] P. Neumayer,[1] C. R. D. Brown,[3,4] P. Davis,[1,5] T. Döppner,[1] R. W. Falcone,[5] D. O. Gericke,[6] G. Gregori,[7] B. Holst,[8] O. L. Landen,[1] H. J. Lee,[5] E. C. Morse,[2] A. Pelka,[9] R. Redmer,[8] M. Roth,[9] J. Vorberger,[6] K. Wünsch,[6] and S. H. Glenzer[1]

[1]*L-399, Lawrence Livermore National Laboratory, P.O. Box 808, Livermore, California 94551, USA*
[2]*Department of Nuclear Engineering, University of California Berkeley, Berkeley, California 94709, USA*
[3]*Department of Physics, Imperial College, London SW7 2AZ, United Kingdom*
[4]*AWE plc., Aldermaston, Reading, RG7 4PR, United Kingdom*
[5]*Department of Physics, University of California Berkeley, Berkeley, California 94709, USA*
[6]*CFSA, Department of Physics, University of Warwick, Coventry CV4 7AL, United Kingdom*
[7]*Department of Physics, Oxford University, Oxford OX1 3PU, United Kingdom*
[8]*Universität Rostock, Institut für Physik, D-18051 Rostock, Germany*
[9]*Institut für Kernphysik, Technische Universität Darmstadt, Darmstadt, Germany*

(Received 24 July 2009; published 10 December 2009)

We present the first ultrafast temporally, spectrally, and angularly resolved x-ray scattering measurements from shock-compressed matter. The experimental spectra yield the absolute elastic and inelastic scattering intensities from the measured density of free electrons. Laser-compressed lithium-hydride samples are well characterized by inelastic Compton and plasmon scattering of a K-α x-ray probe providing independent measurements of temperature and density. The data show excellent agreement with the total intensity and structure when using the two-species form factor and accounting for the screening of ion-ion interactions.

DOI: 10.1103/PhysRevLett.103.245004 PACS numbers: 52.27.Gr

Measurements of the compression and heating of shock-compressed matter are fundamental in the study and understanding of the physical and chemical properties of dense matter at high pressures. Dense matter conditions at >1 Mbar occur in astrophysical objects, such as Jovian planets [1,2] and in inertial confinement fusion experiments [3,4], predicted to compress material to pressures >100 Mbar. Investigation of the behavior of the ionic and electronic properties in this regime is important to determine the equation of state and thermodynamic properties of materials under extreme conditions.

With the use of powerful laser-produced x-ray scattering probes, information on the temperature, density, and ionization state of warm or hot dense matter has been studied [5–7]. In these first experiments from isochorically heated matter, Ly-α and He-α, x-ray sources probed the collective and noncollective plasma regimes. More recently, experiments have characterized shocked-compressed matter [8–10] and measured the coalescence time of multiple shocks traveling through compressed material [10]. This characterization is important for inertial confinement fusion experiments that require a series of well-timed shocks to compress the fuel and ignite thermonuclear burn.

In this Letter, we employ titanium K-α x-rays to characterize compressed matter and present the first ultrafast (10 ps) Thomson scattering measurements [11] as a function of wave vector during shock compression. These laser driven experiments characterize the structure at pressures of several Mbar and determine the thermodynamic properties of LiH targets. In contrast to previous studies [12,13], present measurements of inelastic scattering spectra in the forward and backward scattering regimes provide accurate information on the temperature and density, and further yields the absolute ionic scattering component.

With the use of picosecond diagnostics, sub-ns dynamic material conditions can be probed, avoiding uncertainties due to temporal changes in the structure for shocked systems. We find that the data are sensitive to theoretical models that use the two-species dynamic scattering form factor [7,14–16], and are in best agreement with models that further include screening effects and account for strong ion coupling, i.e., a screened one component plasma (SOCP) model [17] and density functional molecular dynamics (DFT-MD) simulations [18].

Figure 1(a) shows a schematic of the experiment performed at the Titan laser facility, Lawrence Livermore National Laboratory [19]. In these experiments, 300 μm thick solid density LiH foils ($\rho_o = 0.78$ g cm^{-3}) have been compressed and heated by a factor of 2.7 times solid density using a 4 ns shaped laser beam [$I_{\mathrm{PEAK}} = 2.5 \times 10^{13}$ W cm^{-2}, see Fig. 1(c)] that launched a strong shock into the material. An additional petawatt-class short-pulse laser beam, delayed in time by $t = 4.5 \pm 0.3$ ns from the compression beam, was used to create ultrafast Ti K-α x-ray bursts with a temporal resolution of 10 ps [20] and bandwidth of $\Delta E/E = 0.3\%$, that were scattered from the dense compressed plasma. Temporally, spectrally, and angularly resolved Thomson scattering measurements allow

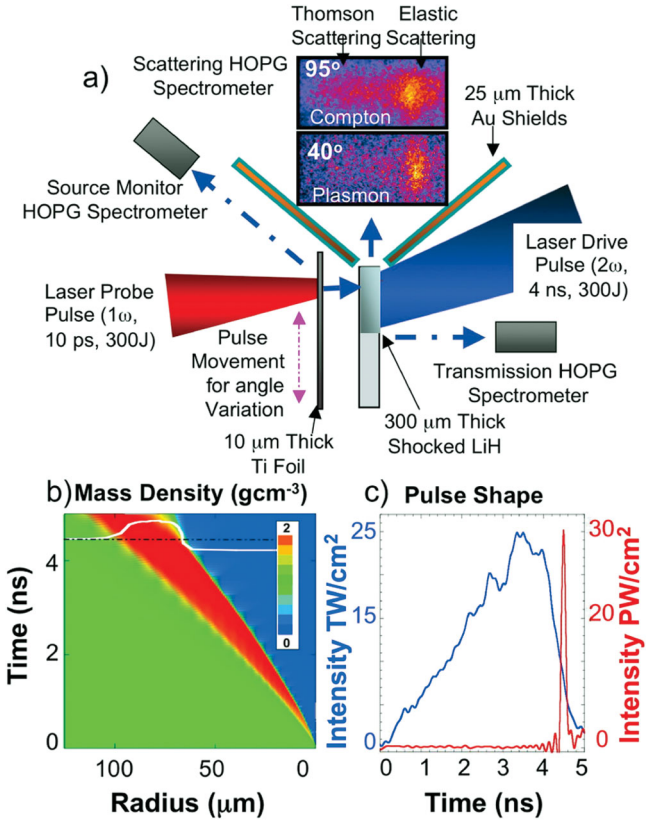

FIG. 1 (color). (a) Schematic of the experimental setup. Here, short-pulse laser produced Ti K-α x rays are scattered from LiH targets that are compressed using a second long-pulse drive beam. Also shown are raw data for scattering at about 95° and 40°. (b) Radiation-hydrodynamic calculations of the mass density, plotted as a function of time and target thickness, where $t = 0$ denotes the start of the drive beam. The predicted compression at $t_0 = 4.5$ ns is about $\rho/\rho_o = 2.7$. (c) Profiles of the measured drive-beam waveform (blue) and a delayed short-pulse beam that was used to create the x-ray probe (red).

characterization of the plasma conditions from elastic and inelastic scattering in the noncollective and collective regimes, i.e., Compton and plasmon features, which were recorded using a high reflectivity [21] curved graphite (HOPG) crystal, [see Fig. 1(a)]. For the conditions in this experiment, shock wave compression and heating of these solid density foils resulted in a Fermi-degenerate plasma, where the width of the Compton feature in the noncollective regime is a measure of the Fermi temperature, providing the electron density of 1.6×1023 cm^{-3}. With the observation of inelastic scattering, the elastic feature, sensitive to the static ion-ion structure factor, can be absolutely calibrated. The temperature, dependent on the total elastic scattering intensity, can then be inferred from the scattering amplitude in the noncollective regime [17], yielding and electron temperature of $T = 1.7$ eV.

The K-α x-ray source was produced from 3.6×10^{16} W cm^{-2} short-pulse laser irradiation of 10 μm thick Ti foils. Approximately 10^{12} photons on target enabled single-shot accuracy, and the source probe energy (4.51 keV) was sufficient to penetrate through the dense plasma. Radiation-hydrodynamic simulations of the mass density, shown in Fig. 1(b), were calculated from the measured heater beam waveforms using the 1D modeling code HELIOS [22]. Calculations predicted electron temperatures ranging from 1.3 to 1.8 eV. The calculated ionization state from radiation-hydrodynamic modeling was $Z = 1$ for conditions at 2.6 to 2.9 times compression, resulting in densities ranging from 1.5–1.7×10^{23} cm^{-3}.

The scattering spectra were measured from the compressed LiH targets at angles ranging from about 35 to 105 degrees, corresponding to $\alpha = 0.45$ to 1.2 where the collective ($\alpha > 1$) and noncollective scattering ($\alpha < 1$) regimes were accessed, probing the electron momentum distribution and electron plasma waves, respectively.

$$\alpha = \frac{1}{k\lambda_S} = \frac{\lambda}{2\pi\lambda_S} \tag{1}$$

Here, k is the magnitude of the scattering vector, where $k = (4\pi E_0/hc)\sin(\theta_s/2)$, and λ_S is the screening length. The parameters θ_s and E_0 are the scattering angle and energy of the incident x-ray probe, respectively. The scattering angle was varied by shifting the short-pulse focus location on the Ti foil with respect to the scattering volume. Accuracy of the pointing resulted in an error of $\pm 10°$ due to the scattering geometry and range of k vectors sampled by the finite exception angle of the spectrometer and the source size.

Figure 2 shows the Thomson scattering measurements in the noncollective regime for a scattering angle of $95 \pm 10°$ and at $t = 4.5 \pm 0.3$ ns after the start of the heater beam. Theoretical fits to the experimental data [17] yield electron densities and temperatures of 1.6×10^{23} cm^{-3} and 1.7 eV, with an error of about $\pm 20\%$ due to noise in the experimental data. Here, we analyze data in the noncollective regime, i.e., large k, where additional error due to temperature dependence on theoretical models is small.

The parabolic Compton feature is downshifted in energy due to the Compton effect by $\Delta E_c = \hbar^2 k^2/2m_e = 43$ eV. The electrons are Fermi degenerate and, in the noncollective regime, the width of the down-scattered peak is proportional to the root of the Fermi temperature, i.e., reflecting the Fermi-degenerate momentum distribution function. The densities inferred from the Compton feature are also consistent with the frequency shift of plasmon scattering at lower k values, providing a direct measure of the electron density. The temperature is inferred from the elastic scattering intensity, calibrated from inelastic scatter, due to its dependency on the static ion-ion structure factor. The ionization state ($Z = 1$), ionization of the $2s$ Li electron, is inferred from collective scattering measurements [10]. Scattering from the dense compressed region dominates the scattering signal, and the contribution to the scattered spectra from uncompressed material, mainly affecting the elastic feature, is subtracted from the spectra

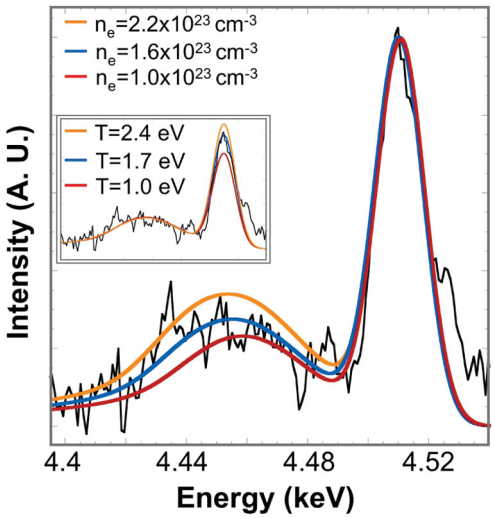

FIG. 2 (color). X-ray Thomson scattering data from shock-compressed LiH targets using Ti K-α x rays in the noncollective scattering regime. The single-shot data at 95 ± 10° show elastic scattering at 4.5 keV and inelastic Compton scattering at 4.45 keV, which allows characterization of the electron density and temperature. Theoretical fits to the experimental data are plotted for various densities and temperatures (inset). Best theoretical fits to the experimental data indicate temperatures and electron densities of 1.7 eV ± 20% and 1.6×10^{23} cm^{-3} ± 20%.

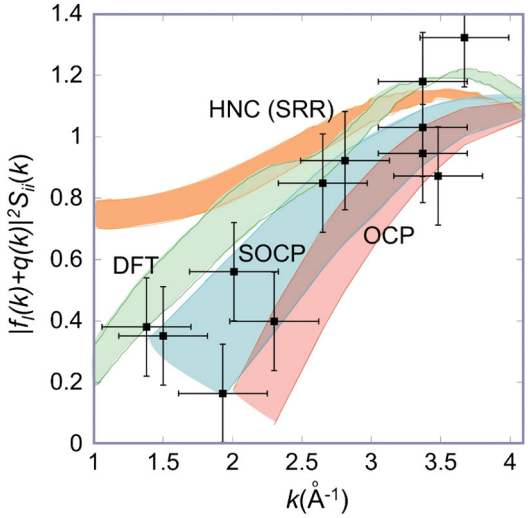

FIG. 3 (color). Measurements of the elastic scattering intensity as a function of the scattering wave vector from shock-compressed LiH targets using Ti K-α x rays (black points) compared to different theoretical models and simulations (see text).

using measured scattering intensities from uncompressed targets. Also, with determination of the electron density from the width of the down-scattered feature, the free-free feature can be absolutely calibrated, $S_{ee}(k = 3.37\ \text{Å}^{-1}) = 0.8$, and the absolute elastic feature can be determined.

Figure 3 shows measurements of the frequency-integrated ion feature of the scattering spectrum, plotted as a function of wave vector. Here the scattered radiation power $P_S(\mathbf{R}, \omega)d\Omega d\omega$ is dependent on the total dynamic structure factor of the electrons $S_{ee}^{\text{tot}}(\mathbf{k}, \omega)$ according to

$$P_S(\mathbf{R}, \omega)d\Omega d\omega = \frac{P_0 r_0^2 d\Omega}{2\pi A} N S_{ee}^{\text{tot}}(\mathbf{k}, \omega) \times d\omega |\hat{\mathbf{k}}_\mathbf{S} \times (\hat{\mathbf{k}}_\mathbf{S} \times \hat{\mathbf{E}}_\mathbf{o})|.^2 \quad (2)$$

The total dynamic structure factor, $S_{ee}^{\text{tot}}(\mathbf{k}, \omega)$ describes the probability of finding a particle with respect to another particle in k space, and includes the elastic scattering feature which is strongly dependent on correlation effects for a strongly coupled plasma [15]

$$S_{ee}^{\text{tot}}(\mathbf{k}, \omega) = |f_I(k) + q(k)|^2 S_{ii}(\mathbf{k}, \omega) + Z S_{ee}^0(\mathbf{k}, \omega) + S_{\text{bf}}(k, \omega). \quad (3)$$

Here, $S_{ee}^0(\mathbf{k}, \omega)$ is the dynamic structure of the free electrons, Z is the ionization states, and $S_{\text{bf}}(\mathbf{k}, \omega)$ is the bound-free feature. The first term is the ion scattering feature for a single-ion species plasma, which describes scattering from tightly bound electrons via the ion form factor, $f_I(k)$, and a screening cloud of valance electrons surrounding the ions via $q(k)$. Here, $S_{ii}(\mathbf{k}, \omega)$ is the dynamic ion-ion structure factor. In this experiment, the ion-acoustic modes cannot be resolved, and the ion-ion structure factor is treated statically, i.e., frequency integrated, where $S_{ii}(\mathbf{k}, \omega) \sim S_{ii}(\mathbf{k})\delta(\omega)$ and $\delta(\omega)$ is the Dirac delta function.

The absolute scattering intensities were compared between shots by measuring the number of source photons produced in each shot, accounting for the source solid angle, and correcting for the HOPG reflectivity dependency on polarization of the incident x-rays [$\cos(2\theta_{\text{Bragg}})$ reflectivity dependence of the p-polarized component [23]]. Also taken into account is the dependency of the scattered power on polarization of the incident radiation for a given scattering angle. For unpolarized light from a laser-plasma source, this dependency is given by $|\hat{\mathbf{k}}_\mathbf{S} \times (\hat{\mathbf{k}}_\mathbf{S} \times \hat{\mathbf{E}}_\mathbf{o})|^2 = \frac{1}{2}[1 + \cos^2(\theta)]$ in Eq. (2).

Also plotted in Fig. 3 are theoretical models for the elastic scattering intensity, dependent on static ion-ion structure factor values, that use the total two-species Chihara formula to calculate the total elastic scattering feature. The band of values for each model are calculated for a range of temperature and density conditions, that account for shot-to-shot variations in the drive-beam waveform and intensity. Here, radiation-hydrodynamic modeling predicts changes in material conditions of $<1\%$ over the probe time, and a uniform compression region is probed by defocusing the drive beam to 750 μm and using a phase plate to smooth the intensity profile [24]. Beam smoothing resulted in a nearly symmetric, flat-top spatial intensity distribution (containing 90% of the energy in the flat top) on target with a fine-scale speckle pattern, i.e., a

speckle width of $<1.5\%$ of the beam diameter. Uncertainties in the measured laser energies are $<5\%$ and uncertainty in the pulse shape measurement system is ± 100 ps.

The SOCP model [17] models the electrons as a neutralizing background and the ions are modeled as linearly screened, charged hard spheres, to account for short-range strong coupling effects. The hyper-netted chain equation model (HNC-Y) uses Yukawa potentials to account for screening effects and short-range repulsion (SRR) was added to the Debye potential as an effective ion interaction potential [25]. Also plotted, are density functional theory (DFT) calculations, coupled with molecular dynamics (MD) simulations [18].

The SOCP calculations use an approximation to the two-species Chihara formula to calculate the ion feature [7], and are in good agreement with experimental data. Calculations that use single-ion species models overestimate the intensity of the scattered ionic feature by a factor of about 1.5 to 3. The total elastic scattering feature [Eq. (3)], when expanded for multiple-ion species plasmas using a charge weighted procedure [17], scales with the average of the square of the number of bound electrons $Z_b^2 = \Sigma N^\alpha (Z_b^\alpha)^2 / \Sigma N^\alpha$. Here, N^α and Z_b^α are the atomic number per molecule and number of bound electrons per species α. Consequently, the ion feature for Li(+)H is smaller than for pure Li(+) at the same electron density. We further observe that the small k-vector behavior is dependent on the approximation to the screening potential. Models that ignore screening effects, such as the one component plasma model (OCP), lie below the data for $k < 3$ Å^{-1}. We find that calculations using the SOCP and OCP models and DFT-MD simulations are in agreement with the measured data, and are in further agreement when screening corrections are applied.

In summary, we have measured the ionic structure of well characterized plasmas using spectrally resolved x-ray Thomson scattering in the collective and noncollective regime. A material compression of 2.7 times solid density was determined from inelastic Compton and plasmon scattering. We find that calculations for the ionic scattering component are sensitive to models that use two-species, and are in best agreement when screening is included. This result validates the use of elastic scattering to infer the ion temperature in dense plasmas. This result is also important for studying equation of state models for materials under extreme conditions, such as those encountered in laboratory astrophysics and in inertial confinement fusion experiments.

This work performed under the auspices of the U.S. Department of Energy by Lawrence Livermore National Laboratory under Contract No. DE-AC52-07NA27344. Work was also supported by the National Laboratory User Facility, Laboratory Directed Research and Development Grants No. 08-ERI-002 and No. 08-LW-004, by the Helmholtz association (VH-VI-104), and by the Deutsche Forschungsgemeinschaft (SFB 652). The work of G. G. was supported by EPSRC Grant No. EP/G007187/1 and the Science and Technology Facilities Council of the United Kingdom. The work of D. G., J. V., and K. W. was supported by EPSRC Grant No. EP/D062837.

[1] H. C. Connolly, Jr. and Stanley G. Love, Science **280**, 62 (1998).
[2] T. Guillot, Science **286**, 72 (1999).
[3] E. I. Moses *et al.*, Fusion Sci. Technol. **47**, 314 (2005).
[4] J. D. Lindl *et al.*, Phys. Plasmas **11**, 339 (2004).
[5] S. H. Glenzer *et al.*, Phys. Rev. Lett. **98**, 065002 (2007).
[6] S. H. Glenzer *et al.*, Phys. Rev. Lett. **90**, 175002 (2003); Phys. Plasmas **10**, 2433 (2003).
[7] G. Gregori *et al.*, J. Quant. Spectrosc. Radiat. Transfer **99**, 225 (2006).
[8] H. J. Lee *et al.*, Phys. Rev. Lett. **102**, 115001 (2009).
[9] E. Garcia Saiz *et al.*, Nature Phys. **4**, 940 (2008).
[10] A. L. Kritcher *et al.*, Science **322**, 69 (2008); Phys. Plasmas **16**, 056308 (2009).
[11] S. H. Glenzer and R. Redmer, Rev. Mod. Phys. **81**, 1625 (2009).
[12] B. Barbrel *et al.*, Phys. Rev. Lett. **102**, 165004 (2009).
[13] D. Riley *et al.*, Phys. Rev. Lett. **84**, 1704 (2000).
[14] J. Chihara, J. Phys. F **17**, 295 (1987).
[15] J. Chihara, J. Phys. Condens. Matter **12**, 231 (2000).
[16] G. Gregori *et al.*, Phys. Rev. E **74**, 026402 (2006).
[17] G. Gregori *et al.*, High Energy Density Phys. **3**, 99 (2007).
[18] K. Wünsch, J. Vorberger, and D. O. Gericke, Phys. Rev. E **79**, 010201(R) (2009).
[19] P. Beiersdorfer *et al.*, in NIFS Proceedings Series No. NIFS-PROC-57 (National Institute for Fusion Studies, Toki, Japan 2004), pp. 40–46.
[20] S. Tzortzakis *et al.*, J. Quant. Spectrosc. Radiat. Transfer **99**, 614 (2006).
[21] F. J. Marshall and J. A. Oertel, Rev. Sci. Instrum. **68**, 735 (1997).
[22] J. J. MacFarlane *et al.*, J. Quant. Spectrosc. Radiat. Transfer **99**, 381 (2006).
[23] Ya. I. Nesterets *et al.*, Phys. Stat. Sol. A **179**, 311 (2000).
[24] S. N. Dixit *et al.*, Opt. Lett. **21**, 1715 (1996).
[25] K. Wünsch *et al.*, Phys. Rev. E **77**, 056404 (2008).